

# Quantification and Three-Dimensional Imaging of the Insulinitis-Induced Destruction of $\beta$ -Cells in Murine Type 1 Diabetes

Tomas Alanentalo,<sup>1</sup> Andreas Hörnblad,<sup>1</sup> Sofia Mayans,<sup>2,3</sup> Anna Karin Nilsson,<sup>2</sup> James Sharpe,<sup>4</sup> Åsa Larefalk,<sup>2</sup> Ulf Ahlgren,<sup>1</sup> and Dan Holmberg<sup>2,3</sup>

**OBJECTIVE**—The aim of this study was to refine the information regarding the quantitative and spatial dynamics of infiltrating lymphocytes and remaining  $\beta$ -cell volume during the progression of type 1 diabetes in the nonobese diabetic (NOD) mouse model of the disease.

**RESEARCH DESIGN AND METHODS**—Using an ex vivo technique, optical projection tomography (OPT), we quantified and assessed the three-dimensional spatial development and progression of insulinitis and  $\beta$ -cell destruction in pancreata from diabetes-prone NOD and non-diabetes-prone congenic NOD.H-2b mice between 3 and 16 weeks of age.

**RESULTS**—Together with results showing the spatial dynamics of the insulinitis process, we provide data of  $\beta$ -cell volume distributions down to the level of the individual islets and throughout the pancreas during the development and progression of type 1 diabetes. Our data provide evidence for a compensatory growth potential of the larger insulin<sup>+</sup> islets during the later stages of the disease around the time point for development of clinical diabetes. This is in contrast to smaller islets, which appear less resistant to the autoimmune attack. We also provide new information on the spatial dynamics of the insulinitis process itself, including its apparently random distribution at onset, the local variations during its further development, and the formation of structures resembling tertiary lymphoid organs at later phases of insulinitis progression.

**CONCLUSIONS**—Our data provide a powerful tool for phenotypic analysis of genetic and environmental effects on type 1 diabetes etiology as well as for evaluating the potential effect of therapeutic regimes. *Diabetes* 59:1756–1764, 2010

From the <sup>1</sup>Umeå Centre for Molecular Medicine, Umeå University, Umeå, Sweden; the <sup>2</sup>Department of Medical Biosciences, Umeå University, Umeå, Sweden; the <sup>3</sup>Department of Disease Biology, Faculty of Life Science, Copenhagen University, Copenhagen, Denmark; the <sup>4</sup>Catalan Institute of Research and Advanced Studies (ICREA), EMBL-CRG Systems Biology Program, Centre for Genomic Regulation, Barcelona, Spain.

Corresponding author: Dan Holmberg, dho@life.ku.dk; or Ulf Ahlgren, ulf.ahlgren@ucmm.umu.se.

Received 21 September 2009 and accepted 26 March 2010. Published ahead of print at <http://diabetes.diabetesjournals.org> on 14 April 2010. DOI: 10.2337/db09-1400.

U.A. and D.H. contributed equally to this article.

© 2010 by the American Diabetes Association. Readers may use this article as long as the work is properly cited, the use is educational and not for profit, and the work is not altered. See <http://creativecommons.org/licenses/by-nc-nd/3.0/> for details.

The costs of publication of this article were defrayed in part by the payment of page charges. This article must therefore be hereby marked "advertisement" in accordance with 18 U.S.C. Section 1734 solely to indicate this fact.

Type 1 diabetes is an autoimmune disorder resulting from the destruction of insulin-producing  $\beta$ -cells by an autoreactive immune response involving CD4<sup>+</sup> and CD8<sup>+</sup> T-cells as well as other leukocyte subsets. Our present understanding of the natural history of type 1 diabetes (1) depends, to a large extent, on analysis of rodent models of the disease, like the nonobese diabetic (NOD) mouse (2). In NOD mice, the development of clinical diabetes is preceded by an inflammation of the pancreatic islets. It is generally thought that an initial event in triggering the development of insulinitis and  $\beta$ -cell destruction is the processing of  $\beta$ -cell antigens by macrophages and dendritic cells residing in the pancreatic islets (3). The antigen-presenting cells are then drained to the pancreatic lymph nodes where they will present the antigen to autoreactive T-cells. In the absence of proper peripheral tolerance mechanisms, this leads to activation and insufficiently controlled expansion of these T-cell clones and eventually to their migration back to the pancreatic islets, where they mediate  $\beta$ -cell destruction (4). While it is well established that the insulinitis progresses over an extended time period, detailed information on the quantification of spatial dynamics is largely lacking, in part, due to limitations in existing technology.

Recently, we have developed an optical projection tomography (OPT)-based approach (5), allowing for ex vivo, global evaluation of molecularly labeled pancreatic constituents (e.g., insulin-producing islet cells or infiltrating CD3<sup>+</sup> T-cells) (6,7). This provides a method for direct quantification and three dimensional-spatial assessment of both infiltrating lymphocytes and remaining  $\beta$ -cell mass during the progression of type 1 diabetes in NOD mice. Using this approach to extract information of islet number,  $\beta$ -cell distribution, and volume down to the level of individual islets throughout the pancreas, we provide a detailed account of the kinetics and spatial extension of the insulinitis and  $\beta$ -cell mass destruction process during the development and progression type 1 diabetes.

## RESEARCH DESIGN AND METHODS

NOD.Bom mice were originally obtained from Bomholtgaard (Ry, Denmark), while NOD.B10-H-2b (NOD.H-2b) mice were kindly provided by Dr. Linda Wicker, (Cambridge University, Cambridge, U.K.). Mice were bred and maintained in the animal facility at Umeå University. All animals were kept on normal diet, and the NOD mice were screened for diabetes by urine analysis for significant glucosuria once a week (BM-test Glucose; Boehringer Mannheim, Mannheim, Germany). Positive results were thereafter verified by daily urine analyses for a week. In our NOD colony, the frequency of diabetes reached 70% in females and 20% in males by 30 weeks of age. All experiments were performed in compliance with the relevant Swedish and institutional laws and guidelines.

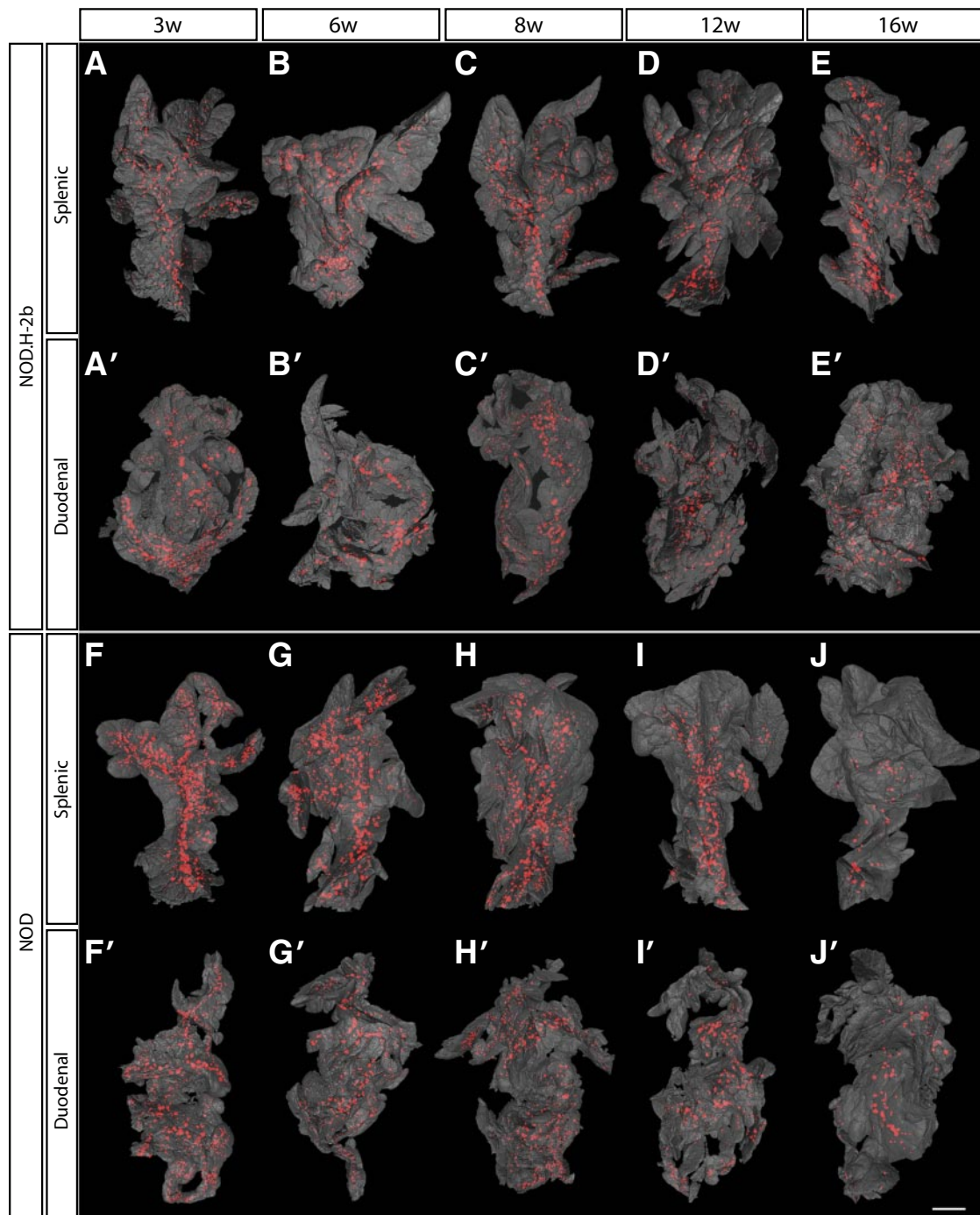


**FIG. 1.** Islet  $\beta$ -cell distribution over time in NOD.H-2b and NOD mice. *A–J'*: Isosurface rendered OPT images of representative NOD.H-2b splenic (*A–E*), duodenal (*A'–E'*), and NOD splenic (*F–J*) and duodenal (*F'–J'*) pancreata labeled for insulin (red). The pancreas outline (gray) is based on the signal from tissue autofluorescence. In contrast to NOD.H-2b mice (*A–E'*), the expected progressive destruction in islet  $\beta$ -cell volume is clearly observed in NOD mice (*F–J'*). Scale bar corresponds to 2.3 mm in *I'*; 2.1 mm in *C*; 2 mm in *D, D', J, J', and G'*; 1.9 mm in *B* and *H*; 1.8 mm in *I* and *H'*; 1.7 mm in *C'* and *E'*; 1.6 mm in *A, E, and F'*; 1.5 mm in *G*; 1.4 mm in *A'* and *B'*; and 1.2 mm in *F*. (A high-quality color representation of this figure is available in the online issue.)

**Organ preparations.** Pancreata from female NOD and NOD.H2-b mice were isolated, stained for insulin, and prepared for OPT scanning, as described previously (6). To minimize variation in the staining procedure, groups consisting of one pancreas at each time point were stained simultaneously. For practical reasons, the gastric and duodenal lobe of the pancreas was scanned as one body (referred to as duodenal) and the splenic lobe as the other. For studies of insulinitis, the same protocols were applied with the addition of Rb anti-CD3 (C7930; Sigma) primary and Alexa 488 anti-Rb (Molecular Probes) secondary antibodies.

**OPT.** OPT scanning using the Bioptronics 3001 OPT scanner (Bioptronics), with exciter D560/40 $\times$  and emitter E610lpv2 filter (Chroma) or exciter D480/30 and

emitter HQ535/50 filter (Chroma) when visualizing Alexa 594 and 488, respectively, was performed as described previously (7). Generation of tomographic reconstructions and quantitations were performed as described previously (7). Iso-surface reconstructions were generated using the visualization software module for Velocity version 4.3.2 (Improvision). To correct for minute-zoom factor aberrations detected in the Bioptronics 3001 OPT scanner, the OPT alignment pin (Bioptronics) was measured with a digital caliper. This value was compared with digital measurements of the (same) scanned alignment pin using SkyScan Software (SkyScan). All measurements were made in triplicate. A correction factor for each magnification was calculated by dividing the value obtained with the caliper measurement by the

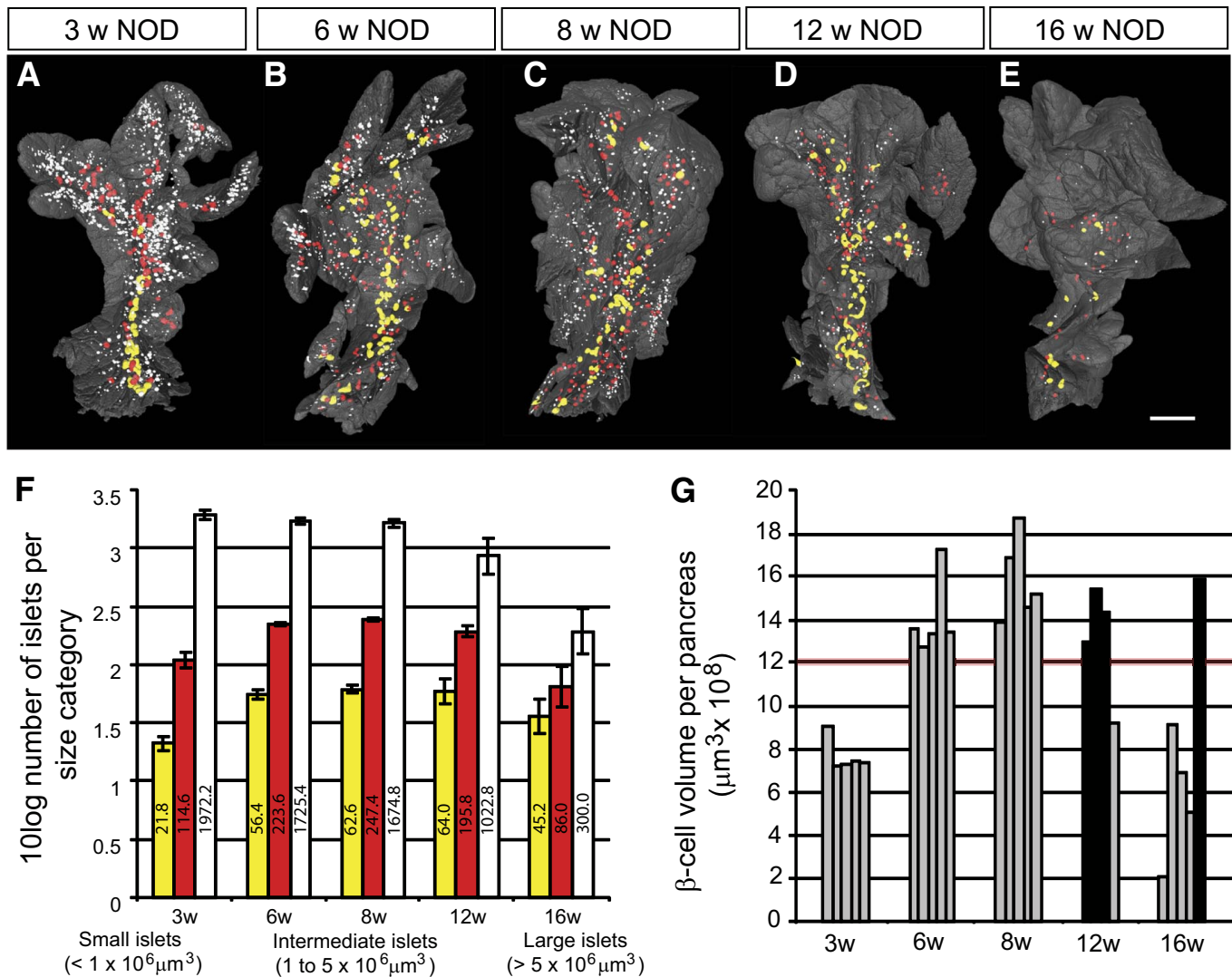


**FIG. 2.** NOD  $\beta$ -cell decay by islet  $\beta$ -cell volume size categories. **A–E:** Isosurface rendered OPT images of representative islet  $\beta$ -cell distributions in 3-, 6-, 8-, 12-, and 16-week-old NOD mice (splenic lobe). Individual islet  $\beta$ -cell volumes are reconstructed based on the signal from insulin-specific antibodies and have been pseudo colored to highlight the distribution of large ( $> 5 \times 10^6 \mu\text{m}^3$  [yellow]), intermediate ( $1\text{--}5 \times 10^6 \mu\text{m}^3$  [red]), and small ( $< 1 \times 10^6 \mu\text{m}^3$  [white]) islets. Scale bar in **E** corresponds to 2 mm in **E**, 1.9 mm in **B**, 1.5 mm in **D**, and 1.2 mm in **A**. **F:** Graph illustrating the progressive loss of Ins $^+$  islets in 3- to 16-week NOD pancreas (duodenal and splenic) broken down to size categories. The values on the *y*-axis corresponds the 10 log value of the average number of Ins $^+$  islets within each size category  $\pm$  SE. The numbers on each bar corresponds to the average number of Ins $^+$  islets within each size category. **G:** Graph illustrating individual variations in total pancreatic  $\beta$ -cell volume in NOD mice at 3, 6, 8, 12, and 16 weeks. Relatively unaffected individuals (black bars) with a total  $\beta$ -cell volume over  $12 \times 10^9 \mu\text{m}^3$  (red line) can be identified at both 12 and 16 weeks.  $n = 5$  for 3, 6, 8, and 16 weeks and  $n = 4$  for 12 weeks. Significance levels for the decay of  $\beta$ -cell volume and number of islets are indicated.  $*P < 0.05$ ;  $**P < 0.01$ . (A high-quality color representation of this figure is available in the online issue.)

value obtained using the SkyScan software. Volume measurements were subsequently adjusted according to the calculated correction factors.

**Immunohistochemistry and morphometric analysis.** Regions of interest (ROIs) containing  $\geq 1$  of the 10 largest islets were identified from the OPT-scanned specimen, as described previously (7). ROIs were isolated, remaining agarose was removed by washing in 0.29 mol/l sucrose at  $57^\circ\text{C}$ , and processed for cryosectioning. Freshly dissected pancreata from 14-week-old female NOD mice were fixed with 4% paraformaldehyde in PBS, washed in PBS, and stored in 30% sucrose at  $4^\circ\text{C}$  before snap freezing in OCT compound (VWR International) and sectioning. Antibodies used were Rb anti-CD3 (C7930; Sigma), Rb anti-phospho-histone H3 (Ser10; Millipore), Rb anti-glucagon (B31-1; Euro-Diagnostica), Rt anti-MadCAM-1 (MECA-89; BD Pharmingen), Rt anti-CD19 (1D3; BD Pharmingen), goat anti-Rb (A11008; Molecular Probes), goat anti-Rb (A11012; Molecular Probes), and goat anti-Rt (A11007; Molecular Probes).

Nuclei covering a total  $\beta$ -cell area of at least  $12,500 \mu\text{m}^2$  were scored from 12- and 16-week-old female NOD and NOD.H2b mice using a grid covering  $2,500 \mu\text{m}^2$ . Average  $\beta$ -cell area was calculated by dividing the total  $\beta$ -cell area by the number of nuclei scored.

**Statistical analyses.** Different zoom factors were used during the OPT scanning to enable imaging of various-sized pancreata (a pancreas at 16 weeks

is approximately four times larger than at 3 weeks). Hence, the smallest detectable object (highest resolution) varies between the largest and smallest pancreas analyzed. To normalize the smallest islet  $\beta$ -cell volume analyzed, between the time series, islet  $\beta$ -cell volumes smaller than the smallest detectable object using the lowest zoom factor were excluded from the statistical analyses. Therefore, only islet  $\beta$ -cell volumes  $> 5,000 \mu\text{m}^3$  were analyzed. This volume corresponds to a spherical object with a diameter of  $\sim 21 \mu\text{m}$ . The excluded islets, even at the highest zoom factor, contributed only marginally to the overall islet number ( $\sim 9\%$  at 3 weeks) and volume ( $< 0.08\%$  at 3 weeks). Subsequent statistical analyses were performed using Excel 2007 software (Microsoft). Mann-Whitney *U* nonparametric (two-tailed) test in SPSS 16.0 (SPSS, Chicago, IL) was used to compare islet numbers and volumes between the different stages. The level of significance was considered to be  $P < 0.05$ . Individual islet  $\beta$ -cell volumes, corresponding spatial coordinates, and tomographic scan data files can be accessed via Web link.

## RESULTS

Pancreata from diabetes-prone NOD mice and non-diabetes-prone NOD.H-2b congenic mice were isolated at differ-



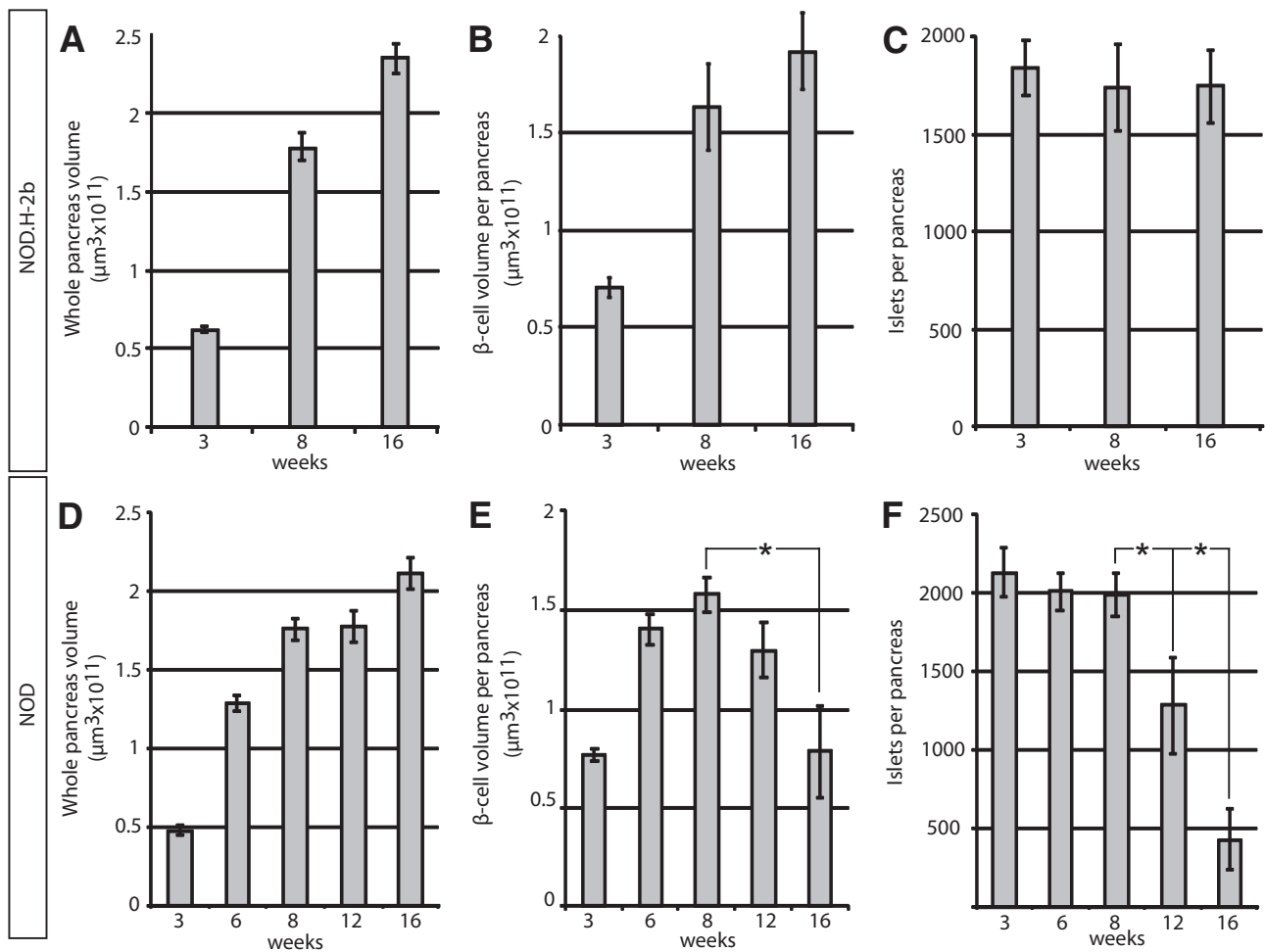


**FIG. 3.** *A* and *D*: Graphs showing the average whole-pancreas volume (duodenal and splenic) at 3, 8, and 16 weeks and in NOD.H-2b mice (*A*) and in NOD mice (*D*) at 3, 6, 8, 12, and 16 weeks. *B* and *E*: Average total pancreatic  $\beta$ -cell volume in NOD.H-2b (*B*) and NOD (*E*) mice. *C* and *F*: Average islet number in NOD.H-2b (*C*) and NOD (*F*) mice.  $n = 5$  for NOD at 3, 6, 8, and 16 weeks,  $n = 4$  for NOD at 12 weeks, and  $n = 3$  for NOD.H-2b at 3, 8, and 16 weeks. Values are given  $\pm$  SE. Significance levels for the decay of  $\beta$ -cell volume and number of islets are indicated. \* $P < 0.05$ ; \*\* $P < 0.01$ .

ent ages, ranging from 3 to 16 weeks; stained with anti-insulin antibodies; and subjected to OPT scanning. In this manner, the volume of insulin-producing  $\beta$ -cells in each individual islet could be directly quantified as well as spatially assessed. As illustrated in Fig. 1, the pancreata from NOD.H-2b mice displayed islets containing insulin-producing  $\beta$ -cells scattered over the whole organ, with a similar pattern observed at all ages studied (Fig. 1A–E). The global assessment of the three dimensional–spatial distribution also confirmed the previous notion (6,8) of an uneven distribution of differently sized islets, with a predominance of small islets in the periphery of the organ and larger islets mainly located centrally in proximity to the large blood vessels and pancreatic ducts (Figs. 1 and 2A–E). The total pancreas volume (Fig. 3A and D) increased over the whole period of observation, with the largest increase occurring between 3 and 8 weeks of age. A similar development was seen in both NOD and NOD.H-2b congenic mice, as illustrated by both strains displaying a similar total pancreas volume at 16 weeks of age (compare Fig. 3A and D). The total  $\beta$ -cell volume increased with similar kinetics (Fig. 3B and E). In contrast, the total number of islets (Fig. 3C and F) had reached adult levels of  $\sim 2,000$  islets at only 3 weeks, agreeing with previous estimates using stereological techniques (9).

These data suggest that the observed increase in  $\beta$ -cell volume between 3 and 8 weeks of age is mainly due to the expansion of already-existing islets rather than through de novo establishment.

In contrast to NOD.H-2b mice, the diabetes-prone NOD mice displayed an expected loss of ins<sup>+</sup> islets due to the autoimmune process, which became evident at  $\sim 8$  weeks of age. Between 8 and 12 weeks of age, the average number of islets decreased by  $\sim 35\%$ , and between 8 and 16 weeks of age the number of islets was reduced by  $>75\%$  (Fig. 3C and F). Interestingly, the drop in islet number was not accompanied by a corresponding drop in total  $\beta$ -cell volume, which was only reduced by  $<20\%$  between 8 and 12 weeks and to  $\sim 50\%$  between 8 and 16 weeks of age (Fig. 3E). This discrepancy could, in part, be explained by the fact that smaller islets were preferentially lost in the earlier stages of the process (Fig. 1F–J). To confirm this notion, we classified all individual islets into size categories arbitrarily chosen to represent “large” ( $>5 \times 10^6 \mu\text{m}^3$ ), “intermediate” ( $1\text{--}5 \times 10^6 \mu\text{m}^3$ ), and “small” ( $<1 \times 10^6 \mu\text{m}^3$ ) islets (Fig. 2) and determined at each time point, the number of ins<sup>+</sup> islets and the mean islet  $\beta$ -cell volume for each of these categories. As illustrated in Fig. 2F, the maximum number of islets in each size category was established at 3 weeks for the smallest category and by 6

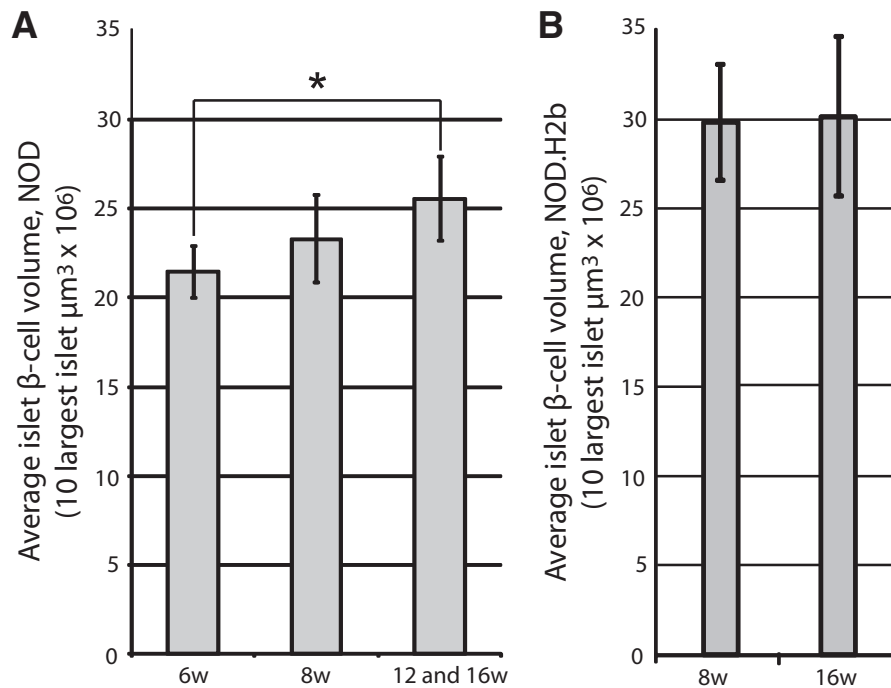


**FIG. 4. A:** Graph showing the average volume of the 10 largest islet-cell volumes in 6- and 8- and 12- and 16-week-old NOD mice (in the latter group only animals with a total pancreatic  $\beta$ -cell volume over  $12 \times 10^9 \mu\text{m}^3$  indicated by filled bars in Fig. 2G were included). The average size of the 10 largest islet  $\beta$ -cell volumes increase from 6 to 16 weeks ( $P = 0.011$ ).  $n = 5$  for 6 and 8 weeks and  $n = 4$  for 12 and 16 weeks. **B:** Graph showing the average volume of the 10 largest islet-cell volumes in 8- and 12- and 16-week-old NOD.H-2b mice.

weeks for the larger categories. Between 8 and 12 weeks, the number of small islets significantly decreased (39%,  $P < 0.05$ ), and between 8 and 16 weeks of age, this reduction was even more prominent (82%,  $P < 0.01$ ). In contrast, the number of intermediate and large islets remained comparatively constant between 8 and 12 weeks. After this point, a clear reduction in the number of intermediate-sized islets was observed at 16 weeks (77% reduction when compared with 8 weeks,  $P < 0.01$ ), while the number of the largest islets, even at this point, only decreased by 28% when compared with those at 8 weeks. Together, these data reveal that the smallest, peripherally located islets are the first to be destroyed during insulinitis induced type 1 diabetes.

The time of onset for diabetes in the NOD mouse is known to display a large individual variation. This is also reflected in the variation in  $\beta$ -cell volume of individual animals. As illustrated in Fig. 2G, the total  $\beta$ -cell volume is kept relatively stable in all animals between 6 and 12 weeks of age, with the exception of one 12-week-old mouse in which a clear reduction was evident. In contrast, four of five 16-week-old mice displayed a similar reduction in  $\beta$ -cell volume, while one mouse appeared relatively unaffected. Diabetes has been suggested to induce  $\beta$ -cell regeneration either through recruitment of progenitor cells from the ductal epithelium or through proliferation of mature insulin-producing  $\beta$ -cells (10–12). It is therefore possible that in addition to a preferential loss of smaller islets, the delay in  $\beta$ -cell volume reduction when compared with the reduction of islet numbers could be a result of  $\beta$ -cell regeneration. We reasoned that if regeneration of  $\beta$ -cells through proliferation, and/or expansion, of mature  $\beta$ -cells would contribute to this phenomenon, the islets remaining in later stages of insulinitis would be predicted to increase in volume. To test this hypothesis, we calculated the average  $\beta$ -cell volume of the 10 largest islets in 6- and

8-week-old mice and compared it with the average of the 10 largest islets in the 12- and 16-week-old mice that did not yet show evidence of reduction in the total  $\beta$ -cell volume (Fig. 2G, filled bars). The average volume of the largest NOD islets increased 19% from 6- to 12- and 16-week-old animals ( $P < 0.05$ ), supporting the notion that regeneration of  $\beta$ -cells is parallel to the autoimmune destruction at this stage of the process (Fig. 4A). The islets in NOD.H2-b mice were larger than in NOD mice at 8 weeks of age, but no increase in the average volume of the 10 largest islets could be observed between 8 and 16 weeks (Fig. 4B). Together, these data indicate that the largest islets possess a potential for compensatory  $\beta$ -cell proliferation and/or expansion to withstand the autoimmune destruction. To test for the possibility that the observed expansion could be due to “swelling” of individual  $\beta$ -cells rather than proliferation, we determined the average  $\beta$ -cell volume in islets isolated from 12- and 16-week-old NOD or NOD.H2-b congenic mice. In both cases, the estimated average  $\beta$ -cell area was similar (NOD 12 weeks:  $85.6 \mu\text{m}^2$ , NOD 16 weeks:  $75.5 \mu\text{m}^2$ , NOD.H2-b 12 weeks:  $76.5 \mu\text{m}^2$ , and NOD.H2-b 16 weeks:  $81.1 \mu\text{m}^2$ ), providing no evidence in support of a hypermorphic alteration of the NOD  $\beta$ -cells.

We next estimated the threshold of total  $\beta$ -cell volume required to withstand the development of overt diabetes (Fig. 5). Five sibling pairs of NOD origin were analyzed at the point when one of the individuals (in each litter) developed overt diabetes, while the other retained normal glucose levels. The diabetic mice displayed consistently lower total  $\beta$ -cell volume when compared with their nondiabetic littermates and confirms our previously reported estimates (6) of a threshold at  $\sim 2.7 \times 10^9 \mu\text{m}^3$ , below which the mice developed clinical diabetes (Fig. 5C). When compared with 16-week-old NOD.H-2b mice, this corresponds to an  $\sim 86\%$  reduction in  $\beta$ -cell volume. These data suggest that the diabetic phenotype of NOD mice

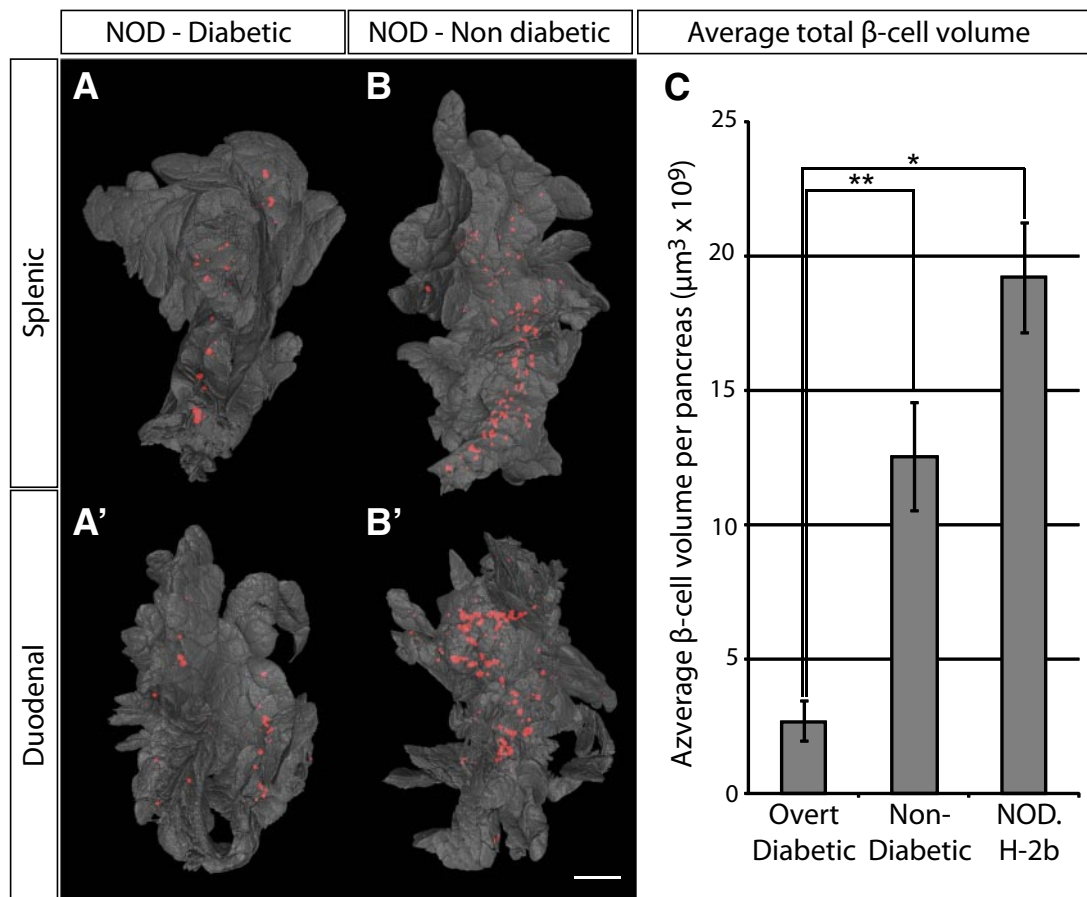


**FIG. 5.** Comparison of overt diabetic and nondiabetic NOD sibling pairs. *A* and *A'*: Isosurface rendered OPT images of representative diabetic (*A* and *A'*) and nondiabetic (*B* and *B'*) splenic (*A* and *B*) and duodenal (*A'* and *B'*) pancreata labeled for insulin (red). The pancreas outline (gray) is based on the signal from tissue autofluorescence. *C*: Graph showing the average total  $\beta$ -cell volume in overt diabetic and nondiabetic NOD sibling pairs ( $n = 5$  for each group, pairs analyzed at 14, 14, 18, 18, and 23 weeks) and in NOD.H 2b mice at 16 weeks ( $n = 3$ )  $\pm$  SE. Scale bar is 2.2 mm in *A*, *B*, and *B'*. Significance levels are indicated, \* $P < 0.05$ ; \*\* $P < 0.01$ . (A high-quality color representation of this figure is available in the online issue.)

develops at a threshold significantly lower than what has been previously reported by point-counting morphometry (13). It is also worth noting that the approximate threshold for development of clinical diabetes established in our study falls well within the estimated interval of a 80–95% reduction in  $\beta$ -cell mass for human type 1 diabetes (14).

We next compared the fluctuations in  $\beta$ -cell volume and islet numbers with the progression of autoimmunity in the NOD mice. Pancreata isolated at the same ages as analyzed above were stained with antibodies against insulin and CD3 to detect  $\beta$ -cells and infiltrating T-cells and were submitted to OPT analysis (Fig. 6). Using this method, we could assess the progression of infiltrating CD3<sup>+</sup> T-cells paralleling the progressive loss of  $\beta$ -cell mass. In agreement with previous observations (15), the first detectable CD3<sup>+</sup>-infiltrating cells were already present in NOD pancreata at 3 weeks of age, progressively increasing in abundance over time. Surprisingly, the preferential depletion of peripherally located islets was not found to coincide with a preferential insulinitis developing in these areas of the organ. Instead, the appearance of the first CD3<sup>+</sup> foci do not appear to occur in any preferred region of the organ; however, to what extent it follows different blood vessels or ducts has not been addressed here. A plausible explanation for this observation is that the destruction of the small islets in the periphery of the organ occurs more rapidly because they contain relatively few  $\beta$ -cells. As a

consequence of this, the  $\beta$ -cell antigen disappears more rapidly and the infiltrating mononuclear cells are no longer retained at the location of the islet. Like unaffected islets, the islets displaying severe insulinitis were surrounded by  $\alpha$ -cells. Thus, while the  $\beta$ -cells eventually were destroyed also in the larger islets affected by insulinitis, no corresponding reduction in  $\alpha$ -cells was observed (Fig. 7).

At later stages, as the individual foci grew in size, the distribution was less evenly spread over the organ, with some areas of large accumulations of infiltrating cells present at the same time as other areas of the organ appearing to be totally unaffected by the inflammatory process. From ~8 to 12 weeks, larger accumulations of CD3<sup>+</sup> cells in direct association with islets became evident. These structures resembled tertiary lymphoid organs (TLOs), with formation of T- and B-cell areas and of high endothelial venules (Fig. 6*F* and *G*), previously reported to be associated with chronic inflammatory diseases (16) including in the NOD mouse (17).

## DISCUSSION

Using a novel tomographic imaging approach to analyze the postweaning development of the pancreas in mice, we have provided detailed three dimensional-spatial and quantitative data regarding the progression of autoimmune-induced insulinitis and  $\beta$ -cell destruction in isolated pancre-



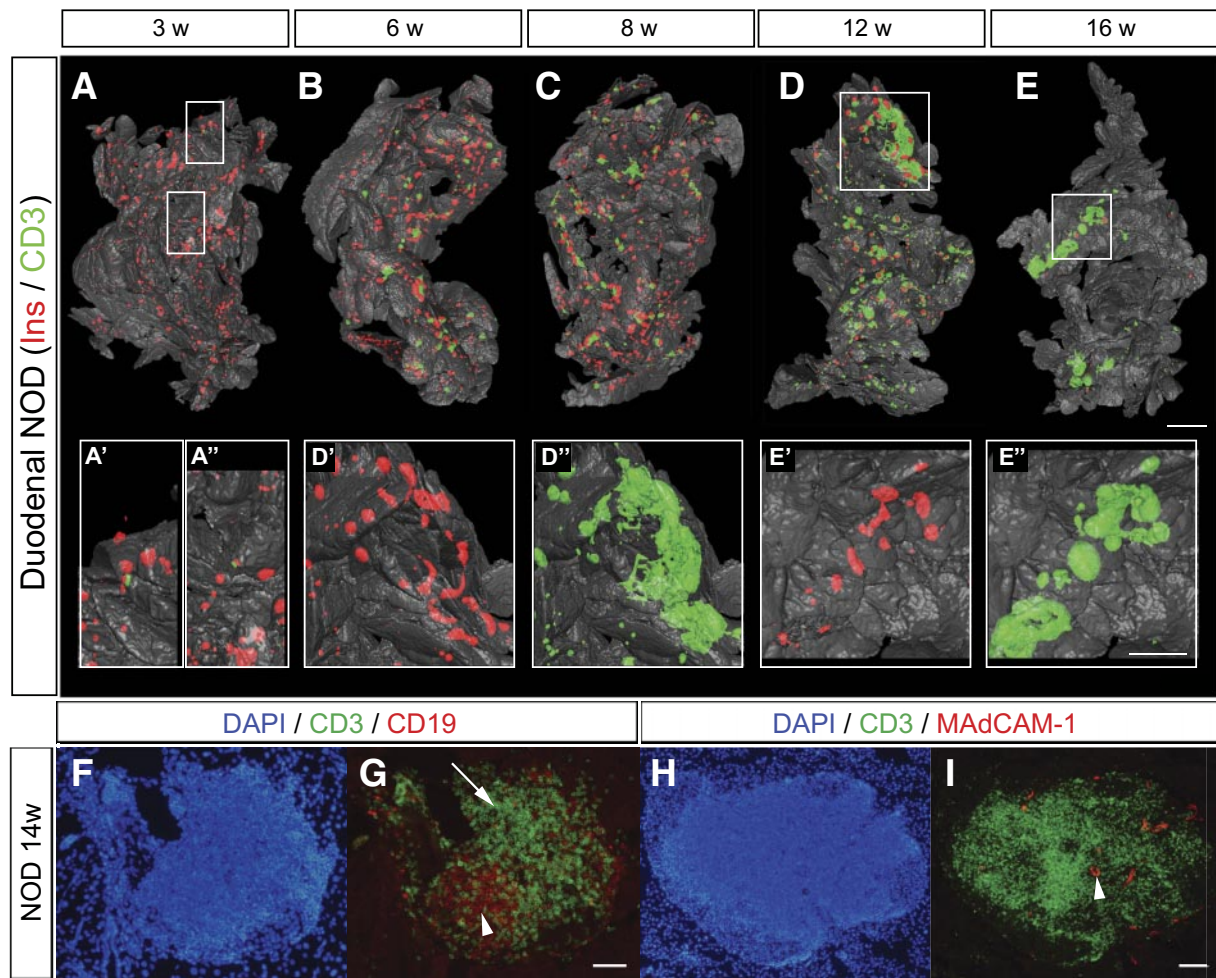


**FIG. 6.** Spatial assessment of the progression of autoimmune insulinitis in the NOD mouse. *A–E*: Isosurface rendered OPT images of representative pancreata (duodenal) from NOD mice at 3, 6, 8, 12, and 16 weeks. Ins<sup>+</sup> islets (red) are reconstructed based on the signal from insulin-specific antibodies and infiltrating T-cells (green) based on the signal from CD3-specific antibodies. *A'–E''*, insets: High-magnification views corresponding to the enclosed boxes in *A*, *D*, and *E*, respectively.  $n = 3$  for 3, 6, 8, and 12 weeks;  $n = 5$  for 16 weeks. Ins, insulin. *F* and *G*: Sections of a pancreata from a 14-week-old female NOD mouse stained with DAPI, anti-CD3 (green), and anti-CD19 (red) (*F*) or anti-CD3 (green) and anti-MAdCAM-1 (red) (*G*). *F*: B-cell areas (arrow head) and T-cell areas (arrow) are indicated by arrow head. *G*: High endothelial venules (arrow head). The scale bar in *E* corresponds to 2 mm in *E*, 1.5 mm in *C*, 1.4 mm in *B*, 1.3 mm in *D*, and 1.0 mm in *A*. The scale bar in *E''* corresponds to 1 mm in *E''*, *E'*, *D'*, *D*, and 0.76 mm in *A'*, *A*. Scale bar in *G* corresponds to 100  $\mu$ m in *F* and *G*. Scale bar in *I* corresponds to 100  $\mu$ m in *H* and *I*. (A high-quality color representation of this figure is available in the online issue.)

ata from the diabetes-prone NOD model three times daily. While this model has been intensively studied using conventional immunohistological methodology, our approach, by enabling directly quantitative and three dimensional-spatial analyses of complete intact organs, gives a more comprehensive picture including a set of novel insights that will aid in understanding the molecular and cellular basis of disease progression in this system.

The observed growth kinetics of the endocrine pancreas in normal mice is not surprising, nor is the progressive loss of  $\beta$ -cell volume observed in the diabetes-prone NOD mice after massive insulinitis has been established. However, the kinetics of the decrease in islet numbers and loss of  $\beta$ -cell volume, together with the finding that the mean  $\beta$ -cell volume of the largest and most resistant islet actually increases, is noteworthy. In fact, this observation provides evidence of a regenerative process simultaneously underway with the autoimmune-induced destruction of  $\beta$ -cells. This has been previously suggested based on the detection of markers associated with  $\beta$ -cell development reoccurring during the autoimmune destruction of  $\beta$ -cells in type 1 diabetes (13). This is also in line with recently reported

findings that abolishment of mature  $\beta$ -cells and insulin expression triggers the regeneration of  $\beta$ -cells mainly due to the expansion of already existing mature  $\beta$ -cells (11). Thus, while we cannot rule out the possibility that the observed expansion of the large islets in the late stage of insulinitis could, in part, be the result of  $\beta$ -cell swelling, these findings support the hypothesis that two competing processes are simultaneously ongoing in the autoimmune type 1 diabetes pancreas, one of autoimmune destruction and the other of regeneration of  $\beta$ -cells. Understanding the basic mechanisms controlling these processes remains an important challenge, with potential implications for interfering and halting the destructive arm of autoimmune diabetes. The observed formation of TLOs in stages of advanced insulinitis may provide a clue for understanding how this is controlled. The role of these structures, which have been reported to appear in various conditions of chronic inflammation (16), could be to sustain autoaggressive insulinitis, tipping the balance in favor of degeneration rather than regeneration of the  $\beta$ -cells. Further insights into when and how these structures are formed in association with insulinitis, together with a better understanding

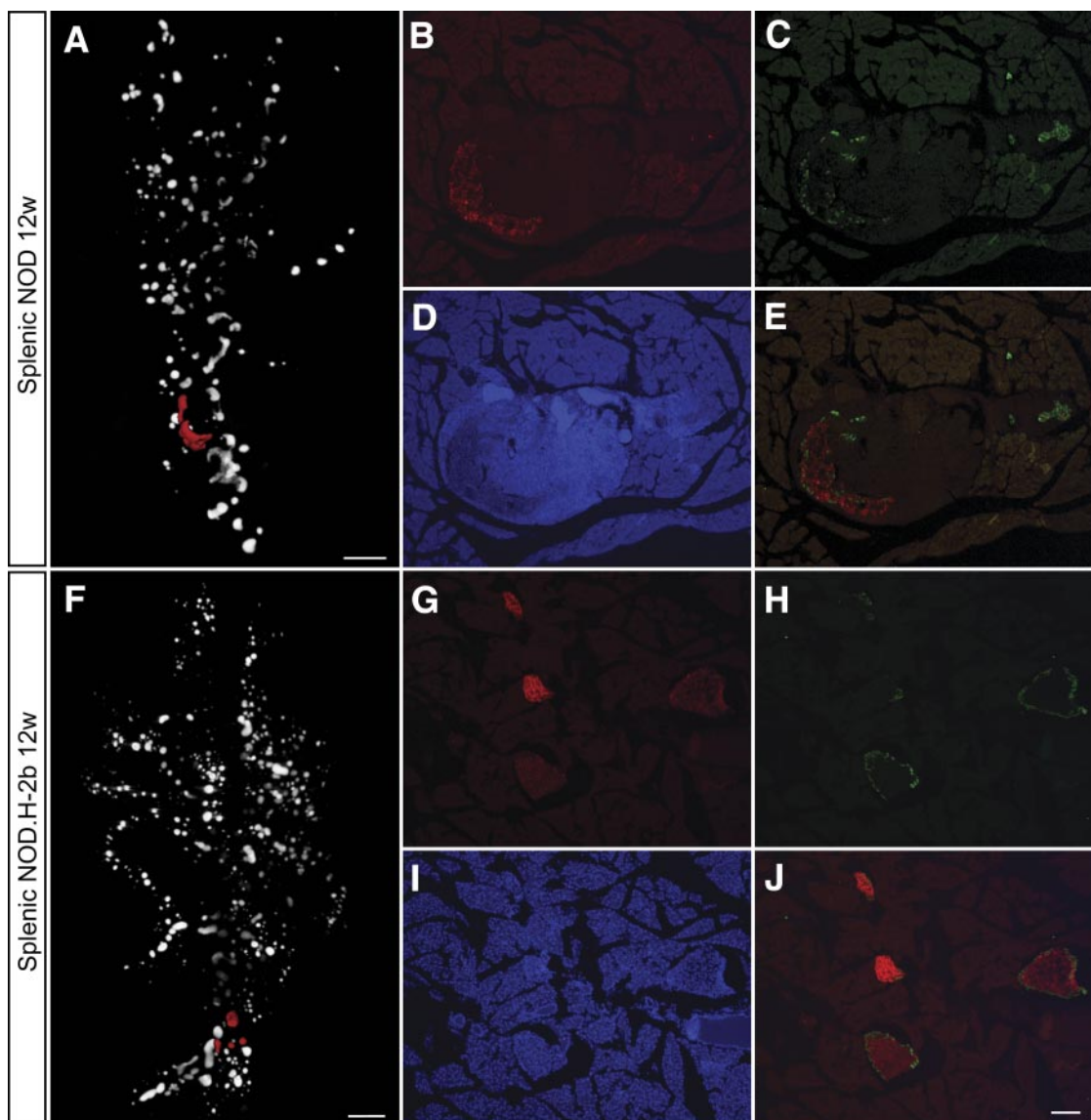


**FIG. 7.** Comparison of  $\alpha$ - and  $\beta$ -cell distribution in 12w NOD and NODH2b mice. *A* and *F*: Volume renderings of  $\beta$ -cell distribution. Cryosections in *B–E* and *G–J* correspond to red pseudocolor in *A* and *F*, respectively. Sections were counterstained against glucagon (*C*, *E*, *H*, and *J*) and DAPI (*D* and *I*). Note the remaining Glu+ cells in the highly infiltrated NOD islets (*C* and *E*). *B* and *G*: Ins+  $\beta$ -cells. Scale bar in *A* and *F* corresponds to 1 mm. Scale bar in *J* corresponds to 100  $\mu$ m in *B–E* and *G–J*. (A high quality color representation of this figure is available in the online issue.)

of their functional contribution to the chronic inflammation, is much warranted and should shed light on how to interfere with the progression of insulinitis and  $\beta$ -cell destruction. Another interesting observation is the unsynchronized spreading of insulinitis into different parts of the organ. In view of the prevailing model for the onset and progression of insulinitis, the observed coexistence of areas with full-blown insulinitis adjacent to areas apparently unaffected by insulinitis is remarkable and suggests that local factors may provide cues for the homing of activated lymphocytes back to the pancreas.

The quantitative and three dimensional–spatial characterization of the autoimmune progression, from the earliest stages of leukocyte infiltration into the endocrine pancreas to the complete destruction of the  $\beta$ -cell volume and development of diabetes, provides a novel and more detailed frame of the process that could be used for elucidating the effect of specific genetic factors (e.g., by comparing NOD mice with transgenic or congenic strains) and for efficient evaluation of various treatment protocols.

#### ACKNOWLEDGMENTS

This work was funded by grants from the Novo Nordisk Fonden, Swedish Diabetes Foundation (to D.H.), the Juvenile Diabetes Foundation, the Swedish Research Council, and the Kempe Foundation (to D.H. and U.A.).

No potential conflicts of interest relevant to this article were reported.

Dr. T. Edlund and I. Jones are acknowledged for helpful comments on the manuscript.

#### REFERENCES

1. Gianani R, Eisenbarth GS. The stages of type 1A diabetes: 2005. *Immunol Rev* 2005;204:232–249
2. Kikutani H, Makino S. The murine autoimmune diabetes model: NOD and related strains. *Adv Immunol* 1992;51:285–322
3. Jun HS, Yoon CS, Zbytniuk L, van Rooijen N, Yoon JW. The role of macrophages in T cell-mediated autoimmune diabetes in nonobese diabetic mice. *J Exp Med* 1999;189:347–358
4. Höglund P, Mintern J, Waltzinger C, Heath W, Benoist C, Mathis D. Benoist, and DMathis. Initiation of autoimmune diabetes by developmentally regu-



- lated presentation of islet cell antigens in the pancreatic lymph nodes. *J Exp Med* 1999;189:331–339
5. Sharpe J, Ahlgren U, Perry P, Hill B, Ross A, Hecksher-Sørensen J, Baldock R, Davidson D. Optical projection tomography as a tool for 3D microscopy and gene expression studies. *Science* 2002;296:541–545
  6. Alantalo T, Asayesh A, Morrison H, Lorén CE, Holmberg D, Sharpe J, Ahlgren U. Tomographic molecular imaging and 3D quantification within adult mouse organs. *Nat Methods* 2007;4:31–33
  7. Alantalo T, Lorén CE, Larefalk A, Sharpe J, Holmberg D, Ahlgren U. High-resolution three-dimensional imaging of islet-infiltrate interactions based on optical projection tomography assessments of the intact adult mouse pancreas. *J Biomed Opt* 2008;13:054070
  8. Hara M, Dizon RF, Glick BS, Lee CS, Kaestner KH, Piston DW, Bindokas VP. Imaging pancreatic beta-cells in the intact pancreas. *Am J Physiol* 2006;290:E1041–E1047
  9. Bock T, Pakkenberg B, Buschard K. Genetic background determines the size and structure of the endocrine pancreas. *Diabetes* 2005;54:133–137
  10. Bonner-Weir S, Weir GC. New sources of pancreatic beta-cells. *Nat Biotech* 2005;23:857–861
  11. Dor Y, Brown J, Martinez OI, Melton DA. Adult pancreatic beta-cells are formed by self-duplication rather than stem-cell differentiation. *Nature* 2004;429:41–46
  12. Halban PA. Cellular sources of new pancreatic beta cells and therapeutic implications for regenerative medicine. *Nat Cell Biol* 2004;6:1021–1025
  13. Sreenan S, Pick AJ, Levisetti M, Baldwin AC, Pugh W, Polonsky KS. Increased  $\beta$ -cell proliferation and reduced mass before diabetes onset in the nonobese diabetic mouse. *Diabetes* 1999;48:989–996
  14. Gepts W, Lecompte PM. The pancreatic islets in diabetes. *Am J Med* 1981;70:105–115
  15. Makino S, Harada M, Kishimoto Y, Hayashi Y. Absence of insulinitis and overt diabetes in athymic nude mice with NOD genetic background. *Jikken dobutsu* 1986;35:495–498
  16. Aloisi F, Pujol-Borrell R. Lymphoid neogenesis in chronic inflammatory diseases. *Nat Rev Immunol* 2006;6:205–217
  17. Hjelmstrom P, Fjell J, Nakagawa T, Sacca R, Cuff CA, Ruddle NH. Lymphoid tissue homing chemokines are expressed in chronic inflammation. *Am J Pathol* 2000;156:1133–1138